Shock Waves (2006) 15:333–340
DOI 10.1007/s00193-006-0032-3

ORIGINAL ARTICLE

Measurement of reflected-shock bifurcation over a wide range of gas composition and pressure

E. L. Petersen · R. K. Hanson

Received: 20 September 2004 / Revised: 17 December 2005 / Accepted: 17 April 2006 / Published online: 14 June 2006

Abstract To determine the extent and magnitude of reflected-shock bifurcation in shock-tube chemistry studies at elevated pressures, experiments were performed using a simple laser schlieren technique and a fast-response pressure transducer. The laser schlieren diagnostic provided a quantitative measurement of the normal-shock passage, an event normally obscured in pressure signals by the bifurcated region. A range of gas mixtures covering molecular weights from 14.7 to 44.0 and specific heat ratios from 1.29 to 1.51 was explored. The results were combined with a standard gas dynamic model to determine the time of arrival of the normal shock wave, the size and strength of the bifurcated region, and the characteristic passage times of dominant features. All results could be expressed in empirical correlations as functions of the gas properties and shock speed. The measured size of the bifurcation zone increased with increasing shock velocity and decreasing specific heat ratio, but displayed no pressure dependence for the conditions of this study ($P_5 = 11 - 265$ atm., $T_5 = 780 - 1740$ K).

Keywords Bifurcation · Shock tube · Reflected shock · Boundary layer

Communicated by F. Lu.

E. L. Petersen (✉)
Mechanical, Materials & Aerospace Engineering,
University of Central Florida,
P.O. Box 162450, Orlando, FL 32816-2450, USA
e-mail: petersen@mail.ucf.edu

R. K. Hanson
Department of Mechanical Engineering,
Stanford University, Stanford, CA, USA

PACS 01.50.Kw · 47.15.Pn

1 Introduction

Depending on the Mach number of the incident shock wave and the gas composition, the interaction between the reflected shock and the boundary layer in a shock tube may lead to boundary-layer separation and bifurcation of the reflected wave (Fig. 1). Bifurcation was first observed in the schlieren images of Mark [1] and Strehlow and Cohen [2] and has since been the subject of much research [3–6]. The contamination of shock-tunnel hot-gas reservoirs via the cold driver gas bleeding through the bifurcation has been a topic of particular interest in reflected-shock studies [7–9]. While modern numerical analyses by Kleine et al. [10], Wilson et al. [11], Nishida and Lee [12], and Daru et al. [13] add much to the understanding and prediction of bifurcation in a shock tube, the original analysis proposed by Mark [1] still provides a simple and reliable description of the flow field [14]. A result common to all studies is that the likelihood of bifurcation increases with the level of diatomic and polyatomic molecules in the test gas mixture.

Although most shock-tube chemistry and spectroscopy experiments avoid bifurcation using a monoatomic bath gas, there is often the need to conduct measurements in mixtures containing realistic collision partners and, therefore, larger fractions of diatomic and polyatomic gases [15]. To better match the conditions of typical combustion devices, such measurements must also be performed at elevated test pressures (> 10 atm.), where the reflected shock wave is interacting with an assuredly turbulent boundary layer [16,17]. The time

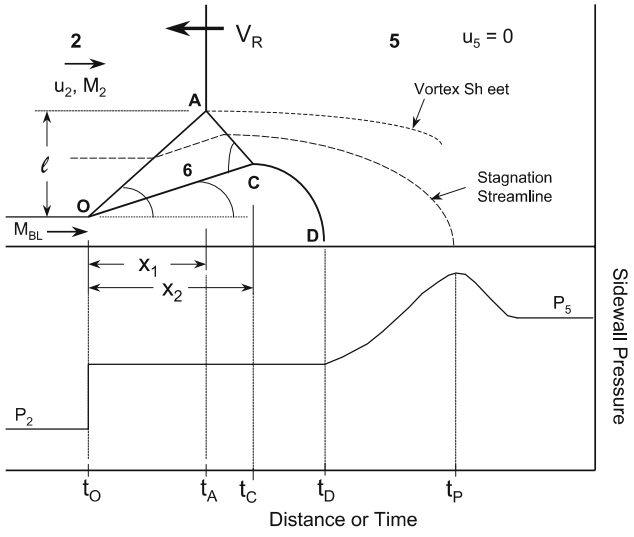

Fig. 1 Model of reflected-shock bifurcation and corresponding sidewall pressure trace. For this ideal depiction, the pressure transducer has zero width and responds instantaneously

scales of the interaction, the size of the bifurcation, and the ensuing effect on the test gas downstream of the reflected shock wave must be known to perform accurate kinetics measurements. However, few quantitative data on the size and duration of typical bifurcation features exist in the literature, and no data at pressures much greater than 1 atm. were found.

In the present study, a simple laser setup and pressure transducer were used to characterize the time and length scales of reflected-shock bifurcation in a high-pressure shock tube. These measurements were combined with a basic gas dynamic model to estimate the extent of the bifurcation. The size (i.e., duration) and corresponding wall static pressures of dominant bifurcation features were correlated as a function of shock strength and gas mixture properties. Provided below is a summary of the theoretical model, followed by a description of the experiments. The results are then summarized and discussed.

2 Theory

When a reflected shock wave interacts with the boundary layer formed behind the incident shock, bifurcation occurs if the boundary layer does not have enough momentum to pass through the normal shock. Figure 1 details the resulting boundary-layer/oblique-shock pattern. The idealized model presented in Fig. 1, originally suggested by Mark [1] and extended by Byron and Rott [18], assumes the energy-deficient boundary-layer gas collects behind the first oblique shock; this occurs when the stagnation pressure in the boundary layer is less than the pressure behind the shock (i.e., $P_{0,\mathrm{BL}}/P_2 < P_5/P_2$). The second oblique shock wave AC returns the flow parallel to the wall. A vortex sheet separates the moving fluid from the stagnant fluid at the endwall [8]. The gas behind the normal portion of the shock wave above point A is assumed to be at reflected-shock conditions per the conventional shock-tube relations. Modern flow visualization techniques such as color schlieren photography [10] produce pictures of the bifurcated flow field that look remarkably similar to the Fig. 1 model.

From the original gas-dynamic model of Mark [1], the Mach number of the boundary layer, M_{BL}, in shock-fixed coordinates is related to the incident-shock Mach number, M_{s}, via

$$M_{\mathrm{BL}} = \frac{2(\gamma-1){M_{\mathrm{s}}}^2 + 3 - \gamma}{(\gamma+1)M_{\mathrm{s}}}\,, \tag{1}$$

where γ is the specific heat ratio of the test gas. Herein, a subscript 1 refers to fill conditions of the test gas, and a subscript 2 refers to conditions behind the incident shock wave. The boundary-layer stagnation pressure is obtained from M_{BL} per the following relations, depending on whether M_{BL} is subsonic or supersonic:

$$M_{\mathrm{BL}} < 1 : \frac{P_{0,\mathrm{BL}}}{P_2} = \left[1 + \frac{(\gamma-1)}{2}{M_{\mathrm{BL}}}^2\right]^{\gamma/(\gamma-1)}; \tag{2}$$

$$M_{\mathrm{BL}} > 1 : \frac{P_{0,\mathrm{BL}}}{P_2} = \left[\frac{(\gamma-1)}{2}{M_{\mathrm{BL}}}^2\right]^{\gamma/(\gamma-1)} \times \left[\frac{2\gamma}{(\gamma+1)}{M_{\mathrm{BL}}}^2 - \frac{\gamma-1}{\gamma+1}\right]^{1/(1-\gamma)}. \tag{3}$$

The reflected-shock pressure ratio, P_5/P_2, can be found from the usual 1D normal-shock relations for shock tubes for a given M_{s} and γ. As $P_{0,\mathrm{BL}}/P_2$ and P_5/P_2 depend only on γ and M_{s}, Mark's theory predicts bifurcation will happen over a limited (γ, M_{s}) region [1].

When bifurcation occurs, the sidewall static pressure distribution through the disturbance is as shown in Fig. 1 [19]. The initial pressure step corresponds to compression downstream of the first oblique shock wave (OA). After the second oblique shock (AC), the pressure again increases and reaches an overshoot condition when the stagnation streamline passes over the measurement station. The final pressure is the endwall pressure, P_5. As seen in Fig. 1, the arrival of the main reflected shock wave is not evident from the sidewall pressure profile alone as the bifurcation disturbance masks the expected pressure increase. This fact led to an additional experimental technique to monitor the arrival of the main reflected shock wave as described below in the

experimental section. The end of the separated region is denoted by the inflection in the sidewall pressure at time t_D.

At the high-pressure conditions of interest, the incident-flow Reynolds number (Re) is greater than typically encountered in lower pressure shock tubes (i.e., $Re/x > 10^7\,\mathrm{m}^{-1}$). The boundary layer becomes turbulent very quickly at these high Re [17,20], further complicating the bifurcation process which heretofore has been studied mainly at lower densities where the boundary layer is laminar for some time [17].

When studying chemistry and spectroscopy behind the reflected shock wave, the arrival time of the normal portion of the shock wave (i.e., t_A), the severity of the bifurcation, and the duration of the flow disruption are important. The height of the collected fluid between the oblique shocks (ℓ) denotes the severity of the disruption. From geometry, the main parameters x_1, x_2, and ℓ can be estimated from

$$x_1 = \Delta t_{AO} V_R \; ; \tag{4}$$

$$\ell = x_1 \tan\theta_1 \; ; \tag{5}$$

$$\frac{x_2}{x_1} = \frac{\tan\theta_1 \tan\alpha + 1}{\tan\delta \tan\alpha + 1} \; , \tag{6}$$

where V_R is the lab-frame reflected-shock velocity as calculated from the shock-tube relations (assumed constant), and x_1, x_2, δ, and θ_1 are defined in Fig. 1. Also, from geometry, $\alpha = \delta - \theta_2 + \pi/2$. Given Δt_{AO} from measurement (i.e., $t_A - t_O$, Fig. 1), Eqs. (4)–(6) can be solved for the lengths x_1, x_2, and ℓ. The angles δ, θ_1, and θ_2 are determined from the oblique and normal-shock relations for given values of M_{BL} and M_R (which are both known for a given M_s, and M_R is the Mach number of the reflected shock wave in shock-fixed coordinates) [8]. The most important of these relations for the calculations herein is the one for the oblique shock angle θ_1, or

$$M_R{}^2 \sin^2\theta_1 = \frac{(\gamma+1)\frac{P_{0,BL}}{P_2} + \gamma - 1}{2\gamma} \; . \tag{7}$$

It should be noted that Eq. (6) is not explicitly needed to determine ℓ from the measurements discussed in the next section but is included herein to indicate how the shock angles and geometry of the bifurcation feature can be obtained if needed.

3 Experiment

Measurements were performed in a 5-cm-diameter, helium-driven shock tube designed for reflected-shock pressures of 1,000 atm. [16]. A bifurcated reflected shock wave was produced using mixtures containing one or more of the following gases: nitrogen, argon, carbon dioxide, methane, helium, and oxygen. Table 1 lists the 10 mixtures utilized and their corresponding volumetric percentages of each constituent, γ_1, γ_2, and molecular weights ($\bar{M}$). The γ_2 values listed in Table 1 are average values for the T_2 range of this study, although they typically varied from the values shown by only ± 0.01. The specific heat ratios defined at T_1 and T_2 were obtained using the Sandia thermodynamic database for the specific heats of the gaseous species as a function of temperature. The usual ideal gas mixture specific heat rules were applied when determining the mixture γ_1 and γ_2 values in Table 1. Also provided in Table 1 are the pressure and temperature ranges studied for each mixture in terms of the reflected-shock conditions. The temperature uncertainties for conditions behind both the incident and reflected shock waves were less than 10 and 20 K, respectively. Errors in the quoted pressure for any experiment were less than 1%. The velocity of the reflected shock wave was calculated from measurements of the incident-shock velocity extrapolated to the endwall using the usual 1D normal-shock relations and the Sandia thermodynamic database.

The characteristics of the bifurcation were determined at a location 20 mm from the endwall using a simple laser diagnostic technique and a fast-response piezoelectric transducer. The laser diagnostic consisted of a cw beam (1-mm dia, < 1 mW) that passed through fused silica optical access ports in the shock tube, perpendicular to the flow direction. A UV-sensitive silicon photodiode monitored the transmitted laser beam intensity. Upon passage of the reflected shock wave, the steep density gradient produces a large change in the refractive index. The net result is deflection and partial extinction (or clipping) of the laser beam, creating a schlieren spike as shown in Fig. 2 from the inverse of the transmitted intensity. This technique is useful as it detects primarily the normal portion of the reflected shock wave. In determining t_A and t_O from the laser extinction trace, t_O is defined as the first step feature due to the deflection of the laser beam (coinciding at the center of the pressure transducer, axially) when the initial oblique wave passes (Fig. 1); t_A is defined by the peak of the main spike, coinciding with the passage of the main normal shock. In the present study, all measurements were conducted using either the output from a frequency-doubled ring-dye laser operating in single mode near 306 nm or a HeNe laser at 632.8 nm.

A fast-response (< 1 μs) PCB 113A pressure transducer ($D = 5$ mm dia) monitored the sidewall pressure. Figure 2 also shows a typical pressure profile in comparison with the transmitted laser intensity (inverse) for a N_2 mixture at $P_5 = 55$ atm. and $T_5 = 1,630$ K. Because

Table 1 Test gas mixtures and range of test conditions employed in the reflected-shock bifurcation measurements

Mixture number	Composition	γ_1	$\bar{M}$	γ_2	P_5 (atm.)	T_5 (K)
1	$50CH_4 + 17O_2 + 33He$	1.40	14.7	1.21	14–20	1,450–1,550
2	$18CH_4 + 12O_2 + 23N_2 + 47He$	1.46	15.1	1.34	47–107	1,270–1,470
3	$75N_2 + 25Ar$	1.44	30.8	1.41	49–87	1,000–1,420
4	N_2	1.40	28.0	1.34	54–61	1,560–1,740
5	CO_2	1.29	44.0	1.20	10–91	780–1,540
6	$60CO_2 + 40He$	1.37	28.0	1.26	12–118	990–1,800
7	$20CH_4 + 13O_2 + 67N_2$	1.38	26.1	1.28	37–148	1,150–1,510
8	$20CH_4 + 13O_2 + 67Ar$	1.51	34.1	1.38	34–265	1,160–1,540
9	$27CH_4 + 18O_2 + 55N_2$	1.37	25.0	1.27	54–194	1,040–1,330
10	$27CH_4 + 18O_2 + 55Ar$	1.46	32.0	1.33	45–128	1,190–1,360

Only mixtures 1 and 3–6 used the laser schlieren technique. Mixture ratios are given in volumetric percentages

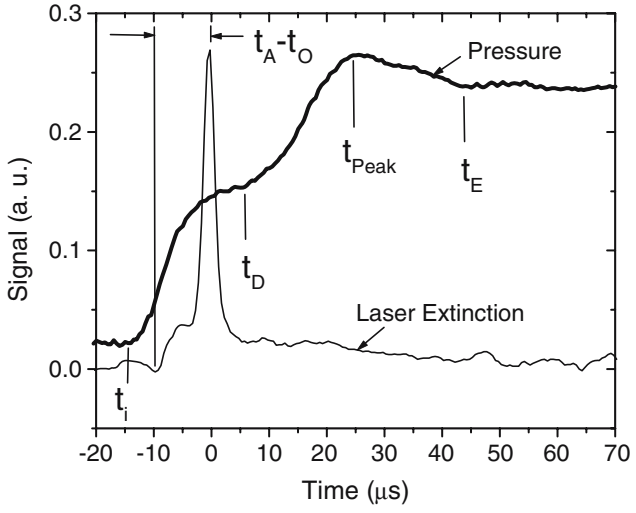

Fig. 2 Transmitted laser intensity (inverse) showing schlieren spike due to the passage of the normal portion of the reflected shock. A comparison with the sidewall pressure is also provided for reference (see Fig. 1). Mixture 4; $T_5 = 1,630$ K; $P_5 = 55$ atm

the reflected shock takes a finite amount of time to pass over the pressure sensor, the measured pressure differs somewhat from the ideal depiction in Fig. 1 and the laser schlieren measurement by the amount of time it takes the leading edge of the bifurcated shock to reach the center of the sensor, or

$$t_0 - t_i = \frac{D}{2V_R} \,. \tag{8}$$

Hence, the time of arrival of the normal portion of the shock wave, t_A, is related to the time of the initial rise in pressure, t_i, via

$$t_A - t_i = \Delta t_{AO} + \frac{D}{2V_R} \,. \tag{9}$$

Equation (9) can be used to determine the time of normal-shock arrival (i.e., time zero) in an experiment containing only pressure data, as in Petersen et al. [15], if an empirical correlation for Δt_{AO} were available. This is the very nature of the current study—to obtain an empirical relation for Δt_{AO}. Note that the rise time of the pressure transducer creates an additional uncertainty but is less than 1 μs in the present study.

4 Results

Measurements of the bifurcation step height ℓ were obtained for mixtures 1 and 3–6 (Table 1) by combining the laser schlieren measurement of Δt_{AO} with Eqs. (4), (5), and (7). The procedure is as follows: (1) obtain Δt_{AO} from the available laser schlieren measurements; (2) calculate x_1 from Eq. (4) and the reflected-shock velocity determined from the 1D shock relations; (3) determine the boundary-layer pressure ratio from Eqs. (1), (2), and/or (3); (4) calculate θ_1 from Eq. (7) using γ for that mixture; and finally, (5) calculate ℓ from Eq. (5). Table 2 provides the available data for the bifurcation height. The results for ℓ can be expressed as a function of the shock speed, the mixture specific heat ratio, and the mixture molecular weight as follows:

$$\ell(\text{mm}) = 7.5 {M_s}^{1.07} {\gamma_2}^{-2.66} \bar{M}^{-0.37} \,. \tag{10}$$

The curve fit for Eq. (10) has a statistical goodness of fit (r^2) of 0.98. This result indicates that the size of the bifurcation zone relative to the tube diameter is a strong function of γ_2, where a smaller γ_2 leads to a larger foot height. Hence, as expected, a larger fraction of di- and polyatomic molecules in the mixture leads to a larger disturbance. Equation (10) shows that ℓ is a weaker function of M_s and $\bar{M}$, but nonetheless increases with increasing shock strength and decreasing molecular weight. Figure 3 presents the measured ℓ data as a function of the empirical correlation. The uncertainty in the estimate of ℓ from the schlieren measurements and

Table 2 Measured results for ℓ and Δt_{AO} from the simultaneous laser schlieren and pressure diagnostics

Mixture number	T_5 (K)	P_5 (atm.)	M_s	ℓ (mm)	Δt_{AO} (μs)
1	1,453	20.3	3.83	6.8	13.0
	1,520	13.8	3.96	7.1	13.3
	1,523	18.6	3.96	7.3	13.7
	1,529	13.8	3.98	7.9	14.5
	1,548	15.2	4.01	7.4	13.5
3	999	86.7	2.37	2.0	4.9
	1,071	62.7	2.48	2.1	5.0
	1,232	55.0	2.72	2.3	5.0
	1,289	54.5	2.80	2.6	5.5
	1,298	55.6	2.81	2.4	5.4
	1,304	48.8	2.82	2.5	5.6
	1,323	50.8	2.84	2.6	5.8
	1,347	55.7	2.88	2.8	6.2
	1,375	52.7	2.92	2.8	6.0
	1,406	54.9	2.96	2.7	5.9
	1,423	52.3	2.98	2.7	5.8
4	1,562	55.4	3.36	3.5	8.1
	1,570	61.1	3.37	3.6	8.1
	1,630	55.4	3.45	3.9	8.1
	1,662	55.8	3.50	3.9	8.7
	1,718	54.9	3.57	3.7	8.8
	1,740	53.9	3.60	4.2	9.0
5	777	11.3	2.62	3.4	20.0
	862	89.0	2.86	3.6	22.1
	959	9.6	3.11	3.9	24.0
	985	77.0	3.18	4.1	25.2
	1,232	7.8	3.77	4.8	28.1
	1,243	71.3	3.79	4.5	26.0
	1,280	91.0	3.87	4.4	25.4
	1,326	38.2	3.97	5.1	29.0
	1,413	59.5	4.15	5.1	28.2
	1,433	31.9	4.20	5.0	27.4
	1,543	51.5	4.42	5.2	27.0
6	994	11.9	2.74	3.1	10.0
	1,182	66.3	3.11	3.7	11.9
	1,296	26.4	3.31	3.8	11.7
	1,377	58.4	3.45	4.1	12.0
	1,378	118.3	3.45	4.1	12.0
	1,519	44.2	3.69	4.5	12.8
	1,551	18.4	3.74	4.7	13.1
	1,798	39.8	4.12	5.3	13.3

Mixtures are per Table 1

the calculations in Eqs. (4) and (5) was approximately ± 0.2 mm. The thickness of the boundary layer at the measurement location was neglected (see below), but this extra height should just be added to the ℓ obtained from Eq. (11).

Similarly, an empirical correlation for the time of normal-shock passage, Δt_{AO}, can be obtained as a function of M_s, γ_2, and $\bar{M}$. Each measurement for Δt_{AO} is listed in Table 2. The resulting empirical expression is

$$\Delta t_{AO}(\mu s) = 4.6 {M_s}^{0.66} \gamma_2^{-7.1} \bar{M}^{0.57} . \quad (11)$$

Equation (11) has an r^2 of 0.985 and is presented in Fig. 4. The time of arrival of the normal portion of the reflected shock wave also increases with increasing shock strength, decreasing specific heat ratio, and increasing molecular weight. The measured value of Δt_{AO} has an estimated uncertainty of ± 1 μs. For the range of conditions of this study (Table 1), the primary angles defining the shape of the bifurcation region, θ_1 and δ, ranged from 36° to 50° and from 11° to 22°, respectively. The location (x_2) and timing (t_{CO}) of the end of the second foot at C can be obtained from Δt_{AO}, θ_1, and the oblique shock relations.

In addition to the size and arrival time of the main bifurcation waves, the duration of the entire event is also important, particularly when the sidewall pressure is a primary diagnostic [15]. The important features of the bifurcation region detectable from the pressure trace

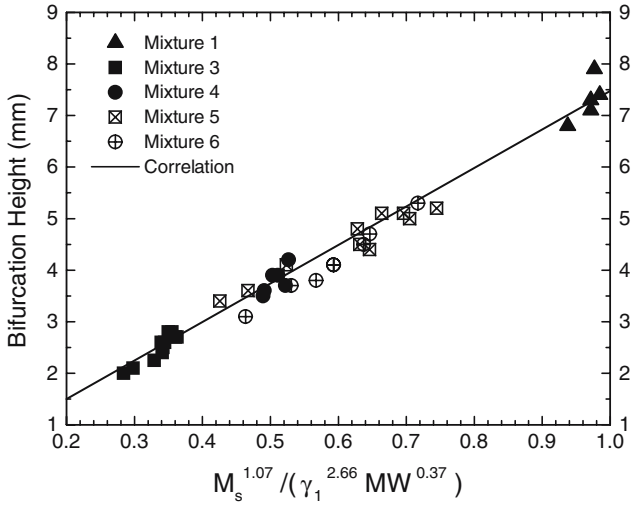

Fig. 3 Correlation of measured bifurcation step height (ℓ). Step height comes from measured Δt_{AO} and Eqs. (4) and (5). *MW* is the mixture molecular weight (i.e., $\bar{M}$)

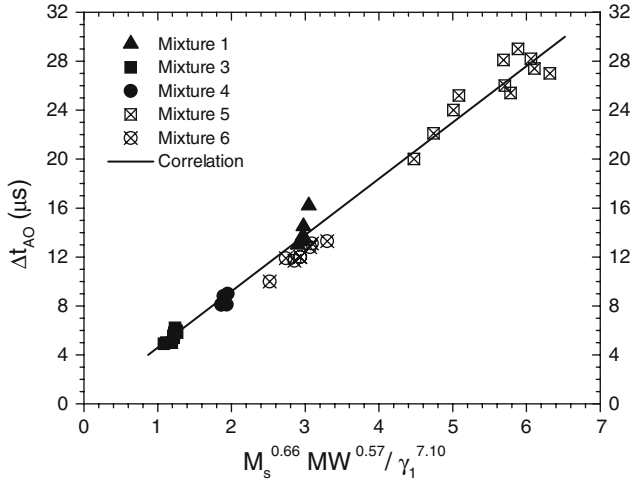

Fig. 4 Correlation of measured normal-shock arrival (Δt_{AO}) for the mixtures (Table 1) where laser schlieren measurements were available. *MW* is the mixture molecular weight (i.e., $\bar{M}$)

(Figs. 1, 2) include the end of the separated region (*D*), the peak pressure, and the complete passage of the disturbance (*E*). Each feature is defined herein relative to the arrival time of the first foot at the measurement location (i.e., the center of the pressure transducer) as in Eqs. (8) and (9), resulting in Δt_{DO}, Δt_{PO}, and Δt_{EO}.

These characteristic times were found to be independent of the shock strength within the accuracy of identifying the primary features in the pressure traces. Hence, an average value of the arrival times was obtained for each mixture over the ranges of temperature and pressure investigated. Table 3 lists the resulting times for all 10 mixtures; in some cases (i.e., for mixtures 2, 3, 5, and 8), the pressure feature at location *E* was not

Table 3 Average pressure-feature times for each mixture

Mixture number	Δt_{DO}	Δt_{PO}	Δt_{EO}
1	33	55	73
2	17	27	–
3	11	22	–
4	21	34	53
5	54	113	–
6	30	60	85
7	27	49	71
8	21	28	–
9	26	56	72
10	24	45	70

All times are in microseconds Mixtures are defined in Table 1

clearly discernable from the pressure traces. The typical uncertainty for each time was ±3 μs for Δt_{DO} and Δt_{PO} and ±5 μs for Δt_{EO}. Each characteristic time was correlated as a linear function of the specific heat ratio upstream of the bifurcation (γ_2) and the mixture molecular weight. The correlations for each are represented by Eqs. (12) –(14):

$$\Delta t_{DO}(\mu s) = 190 - 140\gamma_2 + 0.66\bar{M}; \quad (12)$$

$$\Delta t_{PO}(\mu s) = 425 - 322\gamma_2 + 1.53\bar{M}\,; \quad (13)$$

$$\Delta t_{EO}(\mu s) = 508 - 390\gamma_2 + 2.45\bar{M}\,. \quad (14)$$

The r^2 for each of the above correlations is 0.96 or greater. Figure 5 summarizes the results for each Δt in comparison with their corresponding empirical correlations.

It should be emphasized that the specific heat ratio in Eqs. (10)–(14) is the value behind the incident shock

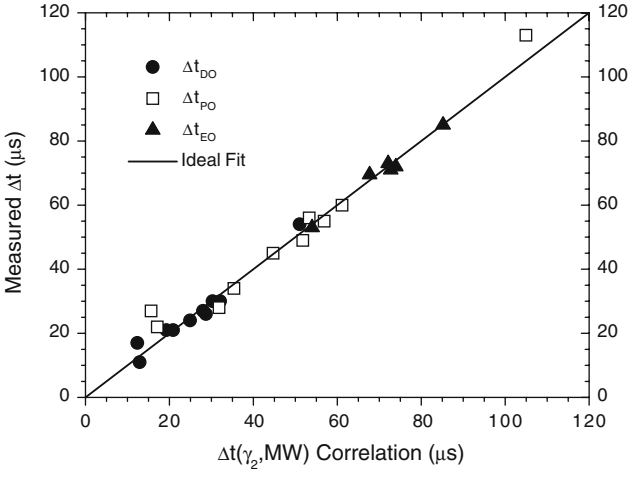

Fig. 5 Measured characteristic times (Δt_{DO}, Δt_{PO}, and Δt_{EO}) compared to the times calculated with their respective correlations [Eqs. (12)–(14)]

wave, i.e., the value upstream of the reflected shock wave, γ_2. This differs from the usual criterion in 1D gas dynamics that γ can be assumed constant. Use of the initial value of γ_1 in the Δt relations did not produce satisfactory correlations ($r^2 < 0.80$) as opposed to the results when γ_2 was used ($r^2 > 0.96$). However, the original 1D theory of Mark [1] still appears valid within the assumptions employed, which assumes $\gamma = \gamma_1$.

5 Discussion

An important application of the above results is the estimation of the extent and magnitude of the bifurcated region for experiments having mixture properties within the range studied (Table 1). From Fig. 3, the height of the disturbance varied from 2 mm up to 8 mm at the test-port location. For a 5-cm shock-tube diameter, the measured ℓ corresponds to 8–32% of the diameter (note that ℓ is doubled to account for the entire perimeter) and therefore 15–54% of the flow area.

The corresponding Δt_{AO} (Fig. 4) ranged from approximately 5 to 30 μs. The arrival time of the normal portion of the reflected shock is important as it signifies the "time zero" for most reflected-shock chemistry and spectroscopy experiments. Using the measured Δt_{AO}, higher precision on the start of the reflected-shock experiment can be obtained. Similarly, the total extent of the disturbance can be estimated from Eqs. (12)–(14) and Fig. 5, where the pressure perturbation caused by the bifurcated region can last up to 100 μs or more for highly polyatomic mixtures.

One important conclusion drawn from the data is that the size and duration of the bifurcated region do not depend on the test pressure for the range of pressures and mixtures of this study. Hence, the results should be generally applicable to both low- and high-pressure shock tubes. Although the basic trends defined by the data are expected to be universal, it should be noted that the magnitude of the results depends on the location of the bifurcated shock relative to the endwall. In the present study, this location was 2 cm. However, the size and extent should vary linearly with distance from the endwall for distances relatively close to the endwall, as in Davies and Wilson [8]. For larger distances from the endwall, others have shown that the variation in foot height grows at a rate much less than the linear distance from the endwall, so care must be taken when extending the present results to other test locations. The results herein should be used as a guide for trends in driven tubes with diameters other than 5 cm and test locations greater than 2 cm from the endwall. Also, the boundary-layer thickness was not considered in the calculation of ℓ from the data. Estimates using an improved boundary-layer theory indicate the boundary-layer thickness at the time of reflected-shock arrival is <1 mm in the shock tube utilized in this study [17].

Several observations can be made regarding chemical kinetics measurements when bifurcation is present. First, as mentioned above, the magnitude and duration of the bifurcation event do not depend on the pressure. Because the bifurcated shock creates a spatially nonuniform flow field, the times for complete passage of the event as correlated herein can be used to gauge the timing of an ideal experiment (suitably corrected for a distance from the endwall other than that employed herein; see above). In the present context, an ideal experiment would be one wherein the pressure perturbation (Fig. 1) has completely passed over the sidewall test location (i.e., after time t_E). In the downstream region, the shocked gas is assumed to be at the conditions determined by the normal-shock relations.

Care should be taken when interpreting kinetics measurements within the flow disruption since the flow field will not be uniform in the transverse direction during this time. Such measurements correspond to fast kinetics at early times after reflected-shock passage. For example, species concentration time histories involving line-of-sight laser absorption should be avoided when the formation/depletion of the species is occurring within the bifurcation event. Measurements at times after passage of the complete flow disruption should be more reliable than those performed while the bifurcation feature is passing.

If interpreting ignition delay times when severe bifurcation exists, one has to consider the true "time zero" as mentioned above. However, the bifurcation should not affect the core portion of the post-shock region, where the gases are at the T_5, P_5 conditions immediately after passage of the normal shock wave. This core region still comprises most of the flow area. Ignition delay times, such as those determined by the authors in previous studies [15], should be unaffected by the presence of a bifurcation feature as long as the results from the temporal diagnostic used to determine ignition (such as pressure and/or species concentration) occur after time t_E.

6 Summary

A series of experiments was conducted in a high-pressure shock tube to characterize the size of the disturbed region when bifurcation of the reflected shock wave occurs. Measurements were performed with a fast-response pressure transducer and a simple laser schlieren

technique over a range of mixture specific heat ratios from 1.29 to 1.51, molecular weights from 14.7 to 44.0, reflected-shock pressures from 11 to 265 atm., and reflected-shock temperatures from 780 to 1,740 K. The data were found to depend strongly on γ and to a lesser extent on $\bar{M}$ and M_s. Empirical correlations were obtained for specific features of the disturbance, including step height and time of arrival of the normal shock, among others.

Acknowledgements The experiments and theoretical modeling were performed at Stanford University while both authors were there, under the support of the Office of Naval Research, with Dr. Richard Miller as the program monitor, and the Army Research Office, with Dr. David Mann as the program monitor. Subsequent analysis and data reduction were performed at The Aerospace Corporation for the Air Force Space and Missile Systems Center under Contract No. F04701-00-C-009 and the University of Central Florida.

References

1. Mark, H.: The interaction of a reflected shock wave with the boundary layer in a shock tube. NACA TM 1418 (1958)
2. Strehlow, R., Cohen, A.: Limitations of the reflected shock technique for studying fast chemical reactions and its application to the observation of relaxation in nitrogen and oxygen. J. Chem. Phys. **30**, 257–265 (1959)
3. Center, R.: Reflected shock interaction with shock tube boundary layers. Phys. Fluids **6**, 307–308 (1963)
4. Dyner, H.: Density variation due to reflected shock-boundary-layer interaction. Phys. Fluids **9**, 879–892 (1966)
5. Honda, M., Takayama, K., Onodera, O., Kohama, Y.: Motion of reflected shock waves in shock tube. In: Kamimoto, G. (ed.) Modern Developments in Shock Tube Research. Proceedings of the 10th International Shock Tube Symposium, pp. 320–327. Shock Tube Research Society, Japan (1975)
6. Fokeev, V., Gvozdeva, L.: Study of bifurcation of reflected shock waves in channels of various cross-sections. In: Kim, Y. (ed.) Current Topics in Shock Waves. Proceedings of the 17th International Symposium on Shock Waves and Shock Tubes, pp. 862–866. AIP, New York (1990)
7. Bull, D., Edwards, D.: An investigation of the reflected shock interaction process in a shock tube. AIAA J. **6**, 1549–1555 (1968)
8. Davies, L., Wilson, J.: Influence of reflected shock and boundary-layer interaction on shock-tube flows. Phys. Fluids Suppl. **I**, I37–I43 (1969)
9. Dumitrescu, L., Popescu, C., Brun, R.: Experimental studies of the shock reflection and interaction in a shock tube. In: Glass, I. (ed.) Shock Tubes. Proceedings of the 7th International Shock Tube Symposium pp. 751–770. University of Toronto Press, Toronto (1970)
10. Kleine, H., Lyakhov, V., Gvozdeva, L., Grönig, H.: Bifurcation of a reflected shock wave in a shock tube. In: Takayama, K. (ed.) Shock Waves. Proceedings of the 18th International Symposium on Shock Waves, pp. 261–266. Springer, Berlin, Heidelberg, New York (1991)
11. Wilson, G., Sharma, S., Gillespie, W.: Time-dependent simulation of reflected-shock/boundary layer interaction in shock tubes. In: Brun, R., Dumitrescu, L. (eds.) Shock Waves @ Marseille I. Proceedings of the 19th International Symposium on Shock Waves, pp. 439–444. Springer, Berlin, Heidelberg, New York (1995)
12. Nishida, M., Lee, M.: Reflected shock/side boundary layer interaction in a shock tube. In: Sturtevant, B., Shepherd, J., Hornung, H. (eds.) Proceedings of the 20th International Symposium on Shock Waves, pp. 705–710. World Scientific, Singapore (1996)
13. Daru, V., Fernandez, G., Tenaud, C.: On CFD to investigate bifurcated shock wave pattern. In: Houwing, F. (ed.) Proceedings of the 21st International Symposium on Shock Waves, Paper 1950 (1997)
14. Takano, Y.: Simulations for effects of side-wall boundary-layer on reflected-shock flowfields in shock tubes. In: Grönig, H. (ed.) Shock Tubes and Waves. Proceedings of the 16th International Symposium on Shock Tubes and Waves, pp. 645–651. VCH, New York (1987)
15. Petersen, E., Davidson, D., Hanson, R.: Ignition delay times of ram accelerator CH_4/O_2/diluent mixtures. J. Prop. Power **15**, 82–91 (1999)
16. Petersen, E.: A shock tube and diagnostics for chemistry measurements at elevated pressures with application to methane ignition. PhD thesis, Stanford University (1998)
17. Petersen, E., Hanson, R.: Improved turbulent boundary-layer model for shock tubes. AIAA J. **41**, 1314–1322 (2003)
18. Byron, S., Rott, N: On the interaction of the reflected shock wave with the laminar boundary layer on the shock tube walls. In: Binder, R., Epstein, M., Mannes, R., Yang, H. (eds.) Proceedings of the Heat Transfer and Fluid Mechanics Institute, pp. 38–54. Stanford University Press, Stanford (1958)
19. Sanderson, R.: Interpretation of pressure measurements behind the reflected shock in a rectangular shock tube. AIAA J. **7**, 1370–1372 (1969)
20. Brun, R., Auberger, P., Van Que, N.: Shock tube study of boundary layer instability. Acta Astro. **5**, 1145–1152 (1978)